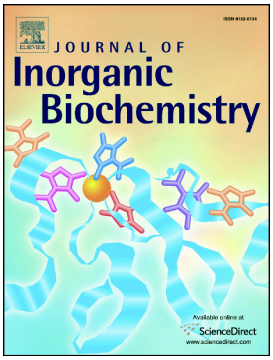


# Unfolding cytochromes c-b562 and Rd apo b562

John J. Kozak, Harry B. Gray, Roberto A. Garza-López

PII: S0162-0134(20)30237-3

DOI: https://doi.org/10.1016/j.jinorgbio.2020.111209

Reference: JIB 111209

To appear in: *Journal of Inorganic Biochemistry*

Received date: 30 April 2020

Revised date: 26 July 2020

Accepted date: 28 July 2020

Please cite this article as: J.J. Kozak, H.B. Gray and R.A. Garza-López, Unfolding cytochromes c-b562 and Rd apo b562, *Journal of Inorganic Biochemistry* (2020), https://doi.org/10.1016/j.jinorgbio.2020.111209

# Unfolding Cytochromes c-$b_{562}$ and Rd apo $b_{562}$

John J. Kozak [a], Harry B. Gray [b] and Roberto A. Garza-López [c]

a) Department of Chemistry, DePaul University, Chicago IL 60604-6116.
b) Beckman Institute, California Institute of Technology, Pasadena, CA 91125
c) Department of Chemistry and Seaver Chemistry Laboratory,
Pomona College, Claremont, CA 91711



## ABSTRACT

We have analyzed the early stages of unfolding of cytochromes c-$b_{562}$ (PDB ID: 2BC5) and Rd apo $b_{562}$ (PDB ID: 1YYJ). Our geometrical approach proceeds from an analysis of the crystal structure reported for each protein. We quantify, residue-by-residue and region-by-region, the spatial and angular changes in the structure as the protein denatures, and quantify differences that result from the seven residues that differ in the two proteins. Using two independent analyses, one based on spatial metrics and the second on angular metrics, we establish the order of unfolding of the five helices in cyt c-$b_{562}$ and the four helices in the apo protein. For the two helices nearest the N-terminal end of both proteins, the ones in the apo protein unfold first. For the two helices nearest the C-terminal end, the interior helix of the apo protein unfolds first, whereas the terminal helix of the holo protein unfolds first. Excluded-volume effects (repulsive interactions) are minimized in turning regions; the overall range in Δ values is Δ=36.3 $Å^3$ for cyt c-$b_{562}$ and Δ=36.6 $Å^3$ for the apo protein, whereas the span for all 20 amino acids is Δ=167.7 $Å^3$. As our work indicates that the interior helix of cytochrome c-$b_{562}$ is the first to fold, we suggest that this helix protects the heme from misligation, consistent with ultrafast folding over a minimally frustrated funneled landscape.

I. Introduction

The pioneering investigations of Wolynes, Saven, and Onuchic [1-5] on funneled energy landscapes as well as definitive experimental work by Dobson, Eaton, and others [6-9] have greatly advanced our understanding of protein folding. Additional insights have followed from research on helical proteins by Thirumalai [10-13] using force fields that depend on the radial and angular orientation of residues to recognize native conformations.

Like Thirumalai, we have been interested in the angle landscapes of helical proteins [14-16]. But our methodology is very different, as we have employed a geometrical approach [14] to analyze these landscapes. We have been particularly focused on heme protein landscapes [9,17-19]. Why are they so different? Why does cyt c-$b_{562}$ fold so rapidly; and more specifically, how is heme misligation avoided as the protein rockets down a minimally frustrated landscape [9]. We have looked more deeply into these landscapes, by characterizing and distinguishing, residue-by-residue and region-by-region, the response of each cytochrome as it unfolds from its native state.

Crystal structures have been reported for cyt c-$b_{562}$ [19] and Rd apo cyt $b_{562}$ [20], providing data for an in-depth study of the respective roles of the metal ion and the hydrophobic region in influencing the unfolding of both proteins. We use the spatial coordinates of cyt c-$b_{562}$ from *E. coli* [19] and those of a redesigned cytochrome, Rd apo $b_{562}$ [20]: cytochrome c-$b_{562}$ has 106 residues, with five helices and a heme; we picked Rd apo $b_{562}$ for comparison, because it also has 106 residues (even though it has an extended turning region and one fewer helix). A principal objective of our study is to characterize the spherical region in the cyt c-$b_{562}$ structure encompassed by residues within a 10 Å radius of the heme (Figure 1).

Figure 1. Structure of cyt c-$b_{562}$ highlighting residues within 10 Å of the heme.

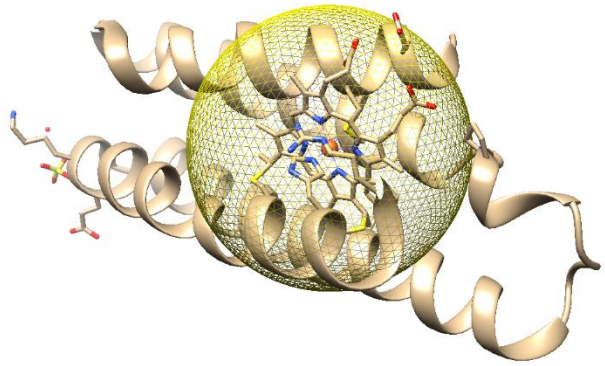

II. Signatures of Unfolding

For each residue i, the coordinates and distance $R_i$ from the crystallographic origin can be determined. Any point can be chosen as the center of a coordinate system, and here we choose the cyt c-$b_{562}$ Fe atom. Numerical values of metrics calculated assuming different origins will, of course, be different, but metrics that depend on the relative difference between two distances, *e.g.* R2 – R1, will be the same. For the apo protein, we choose the origin to be the Fe site in cyt c-$b_{562}$ (Figure 2).

With respect to this common origin, the distance of each residue i is given in Figure 3. The profile for cyt c-$b_{562}$ is displayed in the upper figure, and for the apo protein in the lower one. In both figures, the helix nearest the N-terminal end of each protein is in magenta, the neighboring helix in red. In both figures, the helix closest to the C-terminal end is color coded in cyan, and the neighboring helical region in blue. In cyt c-$b_{562}$, the (fifth) helix between the two N-terminal helices and the two C-terminal helices is in gold. All turning regions are in green. Noticeable is the extended turning (hydrophobic) region, residues 42 to 57, in the apo protein. The magnitude of $R_i$ will depend on the choice of origin; as a result, the vertical scale for the two proteins is different.

Figure 2: Geometrical model for a five-residue segment in cytochrome c-$b_{562}$.

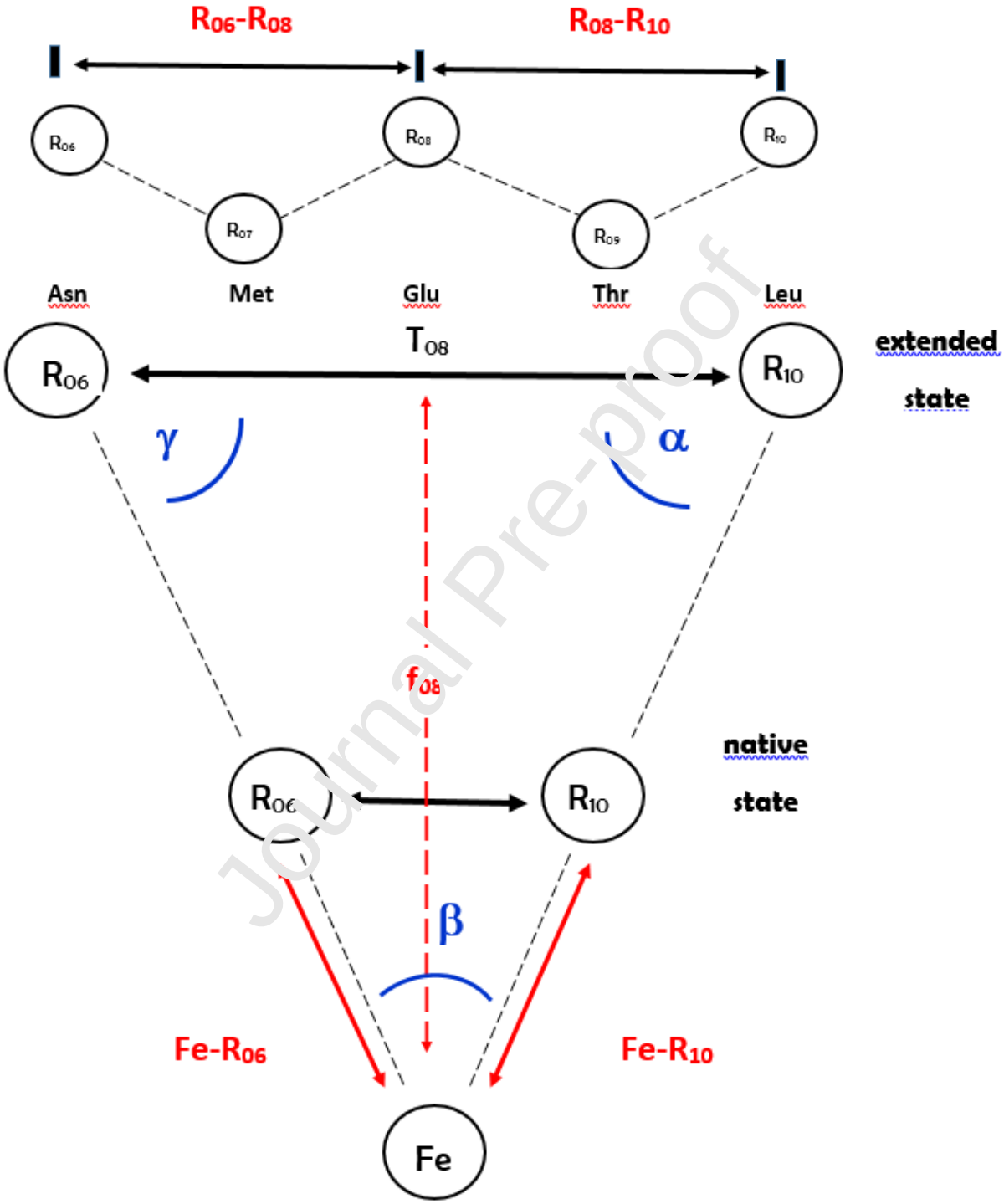






HELIX 1

Figure 3. Distance (Å) of residue i from Fe. Upper /lower figure: cyt c-$b_{562}$/ Rd apo cyt $b_{562}$.

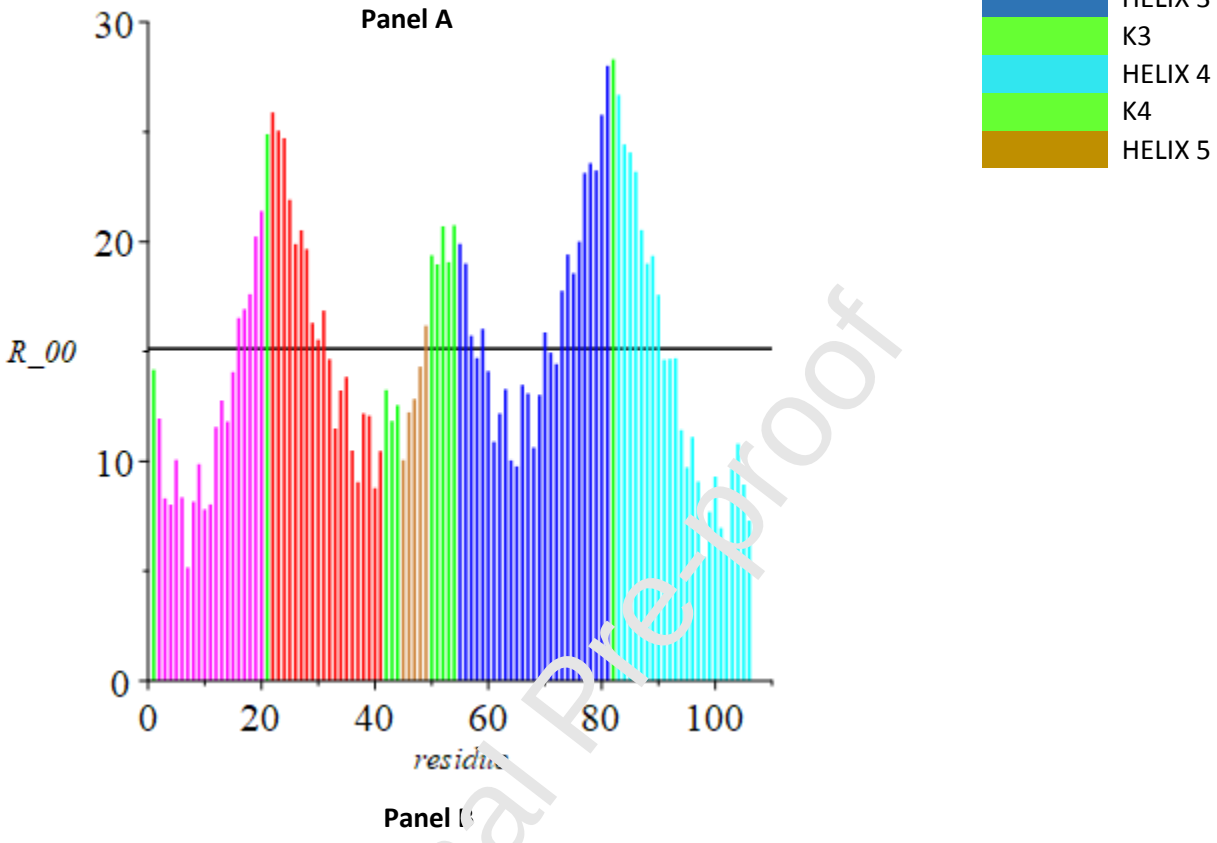

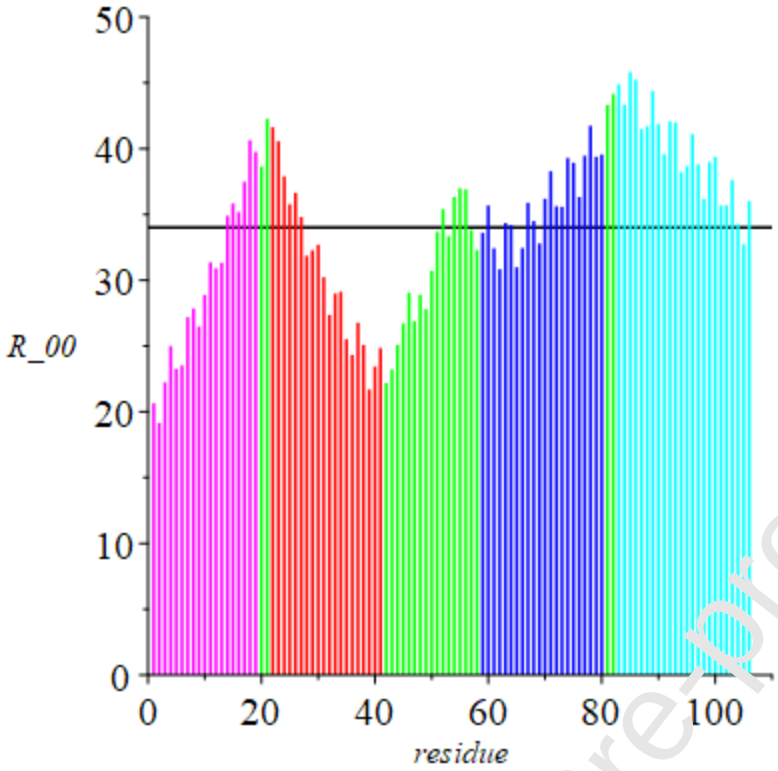


We now introduce two metrics that depend only on the relative distance between two values Ri; these metrics will have the same calculated values irrespective of the choice of origin. We begin by choosing a triplet Ti centered on residue i, *viz*., residues R(i – 1), R(i) and R(i + 1), as our modular unit. Since the crystal structure represents the globally optimized geometry of the native state, this triad captures (exactly) the attractive and repulsive (steric) interactions between and among the three residues in the native state and, once determined from crystal structure data, remains invariant in our approach.

The geometry of a segment of five residues in the first stage of unfolding can be represented by annexing two triads in a *planar* configuration. For example, for a five-residue segment centered on residue i=8, the linear distance T08 between the α-carbons in the terminal residues (i=6 and i=10) of this segment is: T08 = R06to08 + R08to10. A segment of seven residues centered on

residue i=8 in the second stage of unfolding is similarly described as an annexation of three triplets; T08= R05to07 + R07to09 + R09to11. The longest array of triplets considered in this study is a segment of fifteen residues; for i=8 the annexation of seven triplets in a planar configuration is given by

T08 = R01to03 + R03to05 + R05to07 + R07to09 + R09to11 + R11to13 + R13to15.

In the native state, distances between the α-carbons in the terminal residues of each of the above segments can be calculated from crystallographic data. Specifically, in the above example, we have for the five-residue segment centered on residue i=8,

R06to10 = sqrt ((R10x - R6x) $^2$ + (R10y - R6y) $^2$ + (R10z - R6z) $^2$),

for the seven-residue segment,

R05to11 = sqrt ((R11x - R5x) $^2$ + (R11y - R5y) $^2$ + (R11z-R5z) $^2$ ), and for the fifteen-residue segment,

R01to15 = sqrt ((R15x - R1x) $^2$ + (R15y - R1y) $^2$ + (R15z - R1z) $^2$).

We next introduce two metrics using the above defined distances. The first metric is the difference δ in distance (Å) of (here) a five-residue *linear* extension of triplets *minus* the crystallographic distance between terminal α-carbons,

$$\delta\ 08 = T08 - R06to10.$$

Values of $\delta \sim 0$ identify five-residue segments whose geometry is essentially that of the unfolded state, with values $\delta > 1$ reflecting the persistence of the native-state geometry. Thus, for a given helical region, the larger the value of δ, the more the native-state character is conserved.

Complementary to the metric δ is the *ratio* of a n-residue *linear* extension of triplets to the

crystallographic distance between terminal α-carbons in the native state. For a five-residue segment centered on residue i=8,

*ratio* 08 = T08/R06to10.

Values of the *ratio* ~ 1 signal five-residue segments whose geometry is essentially that of the unfolded state; larger values of this ratio signal geometries of five-residue segments different from the unfolded state, reflecting the persistence of native-state regions at this stage of unfolding. Earlier we demonstrated the remarkable result that there is an exact correspondence between values of the *ratio* and the value f of the displacement of residue i from the origin (Fe) relative to the native state f=1 [16]. Hence, values of the *ratio* quantify *both* the persistence of the native-state geometry of the n-residue segment considered *and* the relative displacement of the central residue i in that segment from the heme.

Notice that both metrics depend only on relative distances and remain invariant regardless of the choice of origin of the coordinate system. These metrics are displayed for both proteins in Figures 4 and 5 for a five-residue segment.

Figure 4. Difference (δ in Å) of a 5-residue linear extension of triplets minus the distance between terminal α-carbons (i-2 to i+2). Upper /lower figure: cyt c-$b_{562}$/ Rd apo cyt $b_{562}$

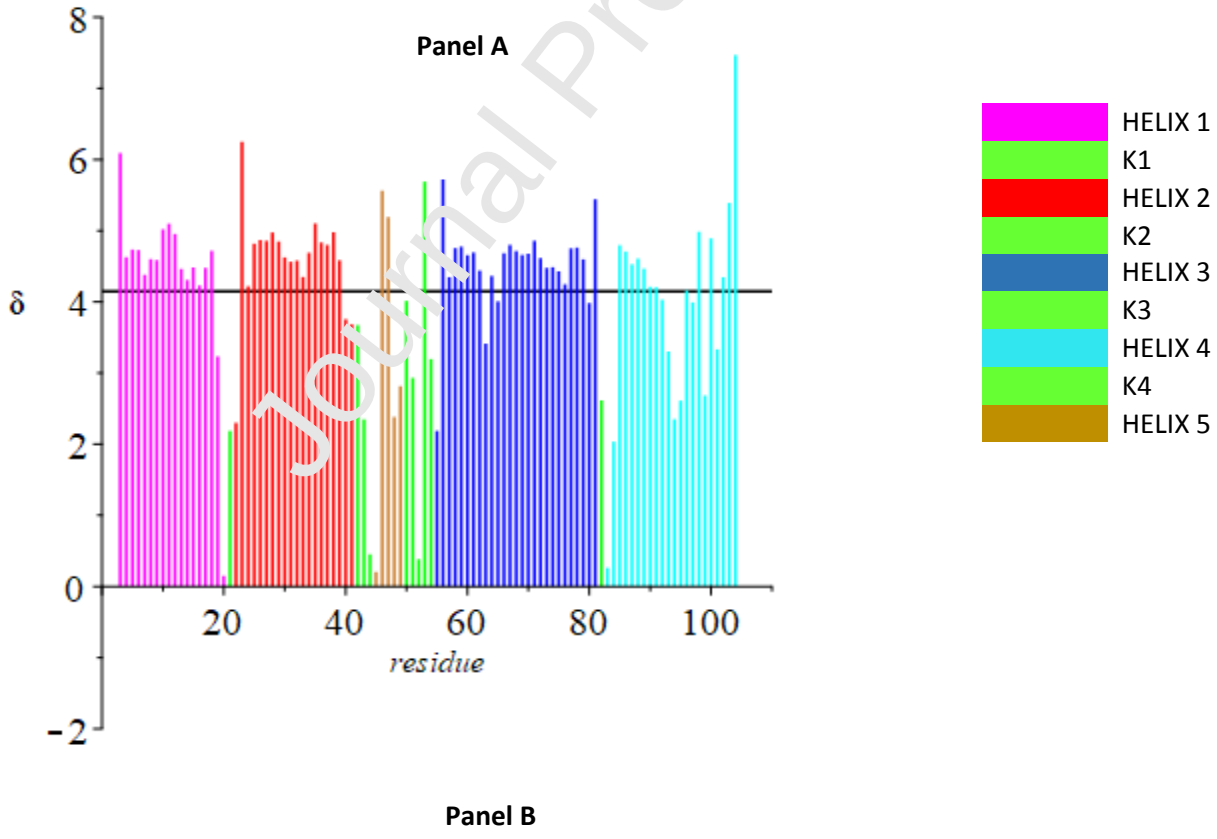

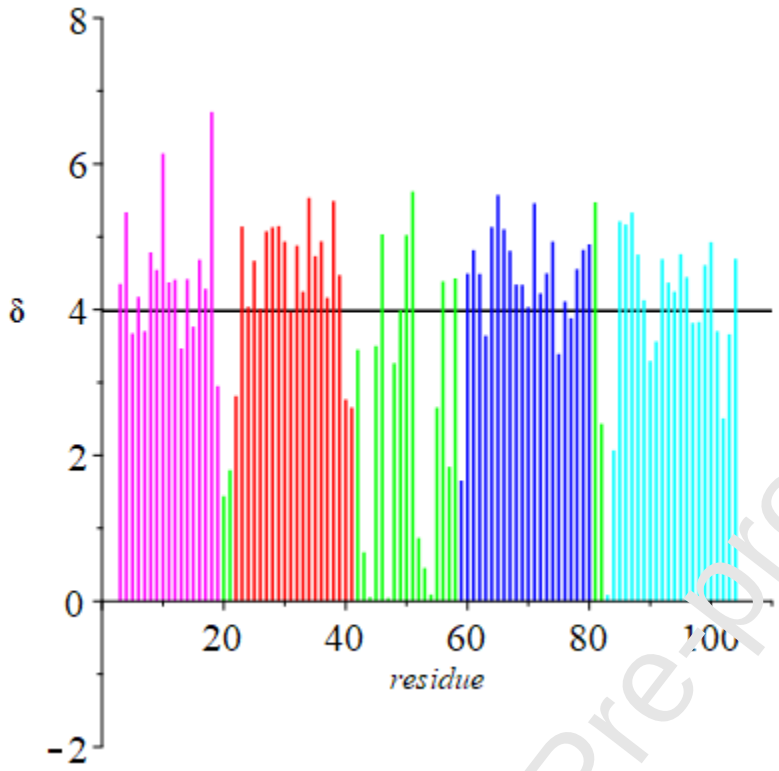


Figure 5. Ratio of a 5-residue linear extension of triplets to the distance between terminal α-carbons (i-2 to i+2). Upper /lower figure: cyt c-$b_{562}$/ Rd apo cyt $b_{562}$.



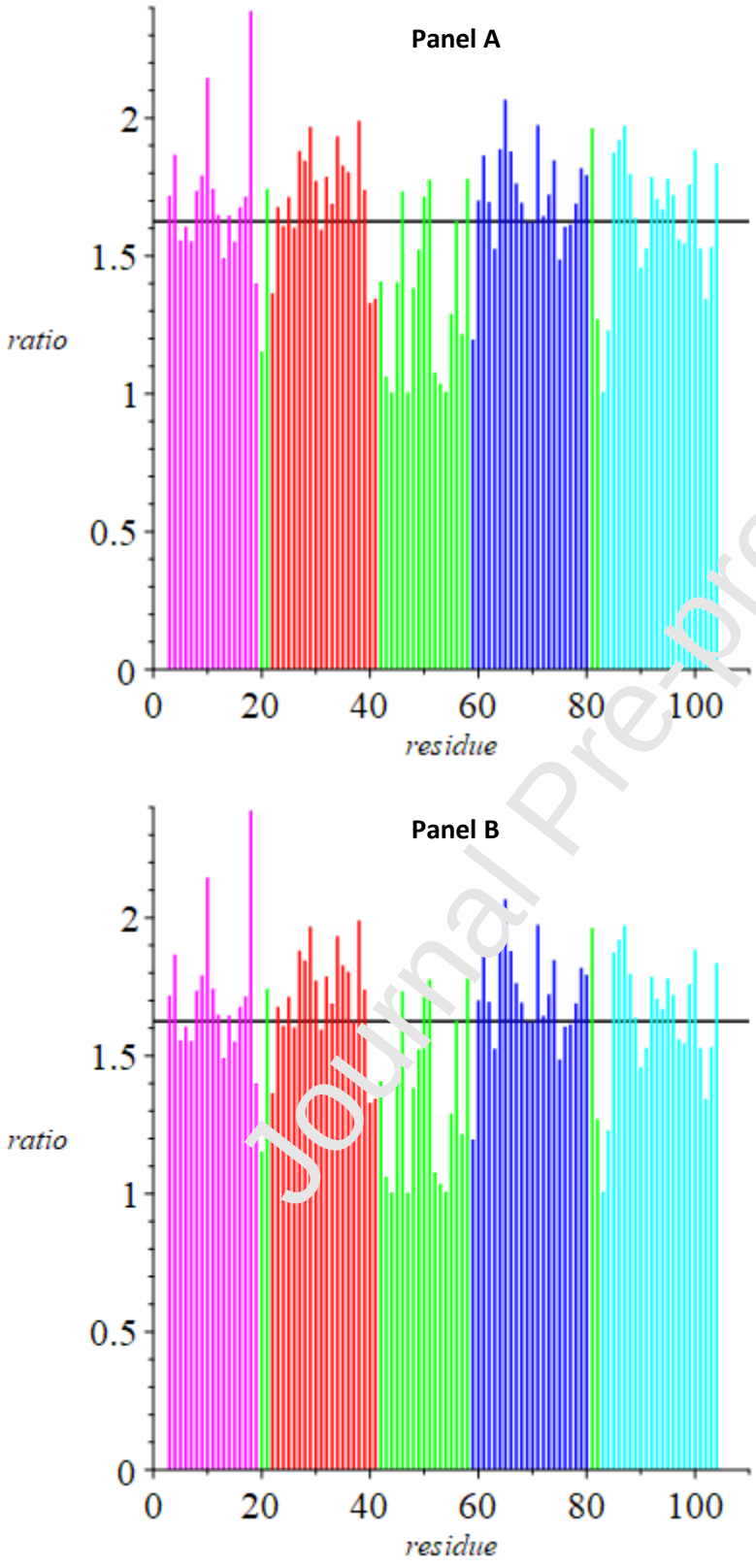

Two observations follow from an examination of the profiles displayed in Figures 4 and 5. First, whereas the profiles in the native state, Figure 3, for each region are sensibly "continuous," those for the first unfolded state are not. Residues nearest turning regions have values of δ and *ratio* noticeably smaller than those in the interiors of helical regions. Second, there are residues in the turning regions that have values δ~0 and *ratio* values ~1. These pivotal residues are identified in Table 1.

**Table 1:** Pivotal residues in turning regions. Data for a five-residue extension

| **Protein** | **Residue** | **Ratio** | **δ distance (Å)** | **Molecular Volume (Å$^3$)** |
|---|---|---|---|---|
| cyt c-$b_{562}$ | ALA 20 | 1.014 | 0.150 | 88.6 |
| | THR 44 | 1.035 | 0.453 | 116.1 |
| | PRO 45 | 1.018 | 0.206 | 112.7 |
| | SER 52 | 1.032 | 0.383 | 89.0 |
| | LYS 83 | 1.024 | 0.252 | 168.6 |
| Rd apo cyt $b_{562}$ | ALA 43 | 1.062 | 0.672 | 88.6 |
| | THR 44 | 1.004 | 0.052 | 116.1 |
| | LYS 47 | 1.004 | 0.043 | 168.6 |
| | SER 47 | 1.077 | 0.867 | 89.0 |
| | PRO 53 | 1.036 | 0.455 | 112.7 |
| | ASP 54 | 1.008 | 0.092 | 111.1 |
| | LYS 83 | 1.008 | 0.086 | 168.6 |

III. Helical Regions

The δ and *ratio* data displayed in Figures 4 and 5 for individual residues can be used to construct average values of those two metrics for each of the helical regions in cyt c-$b_{562}$ and the apo protein. Displayed in Tables A1 and A2 are values of δ for the helical regions for each of the six stages of unfolding; corresponding values of the *ratio* are in Tables A3 and A4.

As can be seen from the comparison presented in Table 2, at every extension except the first (segments of n=5 residues), the helix nearest the C-terminal end of the apo protein unfolds first. For the two interior helical regions, in every case the apo protein unfolds first. For the helix nearest the C-terminal end, except the first, the holo protein unfolds before the apo protein.

Based on this evidence for helices, we anticipate that the apo protein will be the first to denature. The situation when all residues are considered is taken up in the next section.

**Table 2:** Comparison of results for cyt c-$b_{562}$ and the apo protein derived from Tables 3-6. Holo helices in black and apo helices in red. At each extension, H or A denotes the more unfolded helix.

| **Extension (n)** | **H1,H1** | **H2,H2** | **H4,H3** | **H5,H4** |
|---|---|---|---|---|
| 5 | H | A | A | A |
| 7 | A | A | A | H |
| 9 | A | A | A | H |
| 11 | A | A | A | H |
| 13 | A | A | A | H |
| 15 | A | A | A | H |

IV. All-Residue Averages

The *overall* behavior of each protein at each stage of unfolding can be quantified by constructing the average over residues in both helical and turning regions. These averages are presented in Table 3 for S and Table 4 for the ratio. As forecast from the data in Table 2, the systematically smaller values for the apo protein for both metrics suggest that this protein unfolds first.

| Extension | cyt c-$b_{562}$ | Rd apo cyt $b_{562}$ |
|---|---|---|
| 5 | 4.148 | 3.983 |
| 7 | 6.432 | 6.270 |
| 9 | 9.754 | 9.389 |
| 11 | 13.02 | 12.54 |
| 13 | 16.48 | 15.90 |
| 15 | 20.29 | 19.76 |

**Table 3:** Difference δ (in Å) of n-residue linear extension of triplets minus the distance between terminal α-carbons. Average over *all* residues.

**Table 4:** Ratio of n-residue linear extension of triplets to the distance between terminal α-carbons. Average over *all* residues.

| Extension | cyt c-$b_{562}$ | Rd apo cyt $b_{562}$ |
|---|---|---|
| 5 | 1.650 | 1.625 |
| 7 | 1.655 | 1.638 |
| 9 | 1.841 | 1.787 |
| 11 | 1.968 | 1.892 |
| 13 | 2.153 | 2.04 |
| 15 | 2.287 | 2.179 |

V. Angular Phase Diagrams

In earlier work [14-16], we developed angular phase diagrams that provide an independent way of tracking the unfolding of a protein. As noted, the starting point in our approach is a triplet module of three residues, a center residue (i) flanked by its two first nearest neighbors i -1 and i + 1. Adopting a coordinate system in which the iron atom is assigned as the origin, we use crystal structure data to calculate the distance R(i-1) between the iron atom and the α-carbon of the left-most residue, the distance R(i+1) to the right-most residue, and the distance R(i-1) to R(i+1) between the two α-carbons of the terminal residues. Also calculated from crystallographic

data are the angles between R(i-1) and R(i-1 to i+1), R(i-1 to i+1), and R(i-1 to i+1) and R(i+1) , designated α, β, γ, respectively. These signatures were compiled for each of the n residues of the protein. Analogous calculations were carried out for sequences of five, seven, eleven, and fifteen residues [16].

As the protein unfolds from the native state, the angle $\beta_i$ increases, whereas both angles $\alpha_i$ and $\gamma_i$ *decrease* as the protein unfolds. Hence, the behavior of $[\alpha_i, \gamma_i]$ is reciprocal to the behavior of the two spatial metrics [δ, *ratio*], both of which *increase* as the protein denatures. When the protein begins to unfold, there is a reciprocal relation between angular and spatial descriptors.

Data for the spatial metric δ are given in Table A1. To make meaningful comparisons between different helices, average values that differ by ≤ 0.2 Å are regarded as the same. The data show that for the holo protein the native-state geometry of helix H2 near the N-terminal end of the polypeptide chain is *more* conserved than the terminal helix H1, while the angular phase-diagram data reported in [16] revealed that this is accompanied by a *greater* percent departure of angles $[\alpha_i, \gamma_i]$ from the native state for helix H1 than for H2.

This reciprocity also is displayed by the two helices H4 and H5 nearest the C-terminal end in the holo protein; the spatial descriptor δ documents that the native-state geometry of helix H4 is *more* conserved than the terminal helix H5, while the percent departure of angles $[\alpha_i, \gamma_i]$ from the native state is *greater* for H5 than for H4. The single exception is the last (sixth stage) of unfolding. The signature $[\alpha, \gamma]$ for the holo protein was given in [16]. This signature for Rd apo cyt $b_{562}$ is in Figure 6.

Figure 6. Percent departure of helical and non-helical regions from the native state [α,γ] domain for Rd apo cyt $b_{562}$.


Using the data for δ in concert with the [α, γ] signatures for Rd apo cyt $b_{562}$, we find *exactly* the same behavior for H1, H2 for the apo protein as for the holo protein, not a surprising result since the only residue different in the two proteins is residue 7 in the helix nearest the N-terminal end. However, for the two helices nearest the C-terminus, the similarity is not conclusive, as five residues are different in one helix (residues 98, 99, 101,102 and 106).

## VI. Discussion

The behavior of turning regions and the role of the Fe atom as the heme protein unfolds have been documented in this study. Displayed in Table 5 is the average distance difference δ and *ratio* in the extended turning region in Rd apo cyt $b_{562}$, residues 42-57. Compared with the helical regions in the apo protein, the [δ, *ratio*] values for this turning region are *smaller* in the first three stages of unfolding but *larger* in the last three stages.

**Table 5:** Average ratio and distance difference δ (in Å) in the extended non-helical (turning) region (residues 42-57) in Rd apo cyt $b_{562}$.

| Extension (n) | Ratio | Difference Distance (Å) |
|---|---|---|
| 5 | 1.329 | 2.560 |
| 7 | 1.494 | 5.550 |
| 9 | 1.615 | 8.741 |
| 11 | 1.805 | 12.62 |
| 13 | 1.990 | 16.92 |
| 15 | 2.294 | 21.09 |

Smaller values of these metrics signal that the turning region is more unfolded than helical regions, whereas larger values suggest that the turning region is less so. This "crossover" behavior is a consequence of the fact that H-bonds in the neighboring helices (H2, H3) are disrupted in going from the first stage of unfolding to the sixth stage. One turn of a helix involves 3.6 residues, two turns involve 7.2 residues, three turns 10.8 residues, and four turns 14.4 residues. The first stage of unfolding (5-residue segments) disrupts one turn of the helix, the third stage (9-residue segments) disrupts two turns, the fourth stage (11-residue segment) disrupts three turns and the sixth stage (15-residue segments) disrupts four turns. The crossover occurs when three turns of the helix are disrupted in the two helices bracketing the turning region.

The pivotal residues identified in Table 1 are turning points separating regions. The average molecular volume ($Å^3$) of n-residue segments centered on each residue are given in Table 6. Values are reported for each stage n of unfolding, so neighborhoods capturing successively larger numbers of nearest neighbors are involved.

**Table 6:** Average molecular volume (Å3) of n-residue segments centered on residue i. Δ is the maximum difference of molecular volume values for all neighborhoods centered on residue i.

| **Protein** | **Residue i** | **n=5** | **n=7** | **n=9** | **n=11** | **n=13** | **n=15** | **Δ(Å$^3$)** |
|---|---|---|---|---|---|---|---|---|
| | | | | | | | | |
| **cyt c-b$_{562}$** | ALA 20 | 88.6 | 122.8 | 124.2 | 125.2 | 128.8 | 133.8 | 45.2 |
| | THR 44 | 116.1 | 105.8 | 119.7 | 130.2 | 128.7 | 130.1 | 24.4 |
| | PRO 45 | 112.7 | 113.8 | 119.7 | 133.4 | 128.7 | 130.1 | 20.7 |
| | SER 52 | 89.0 | 123.4 | 118.5 | 117.1 | 127.8 | 134.8 | 45.8 |
| | LYS 83 | 168.6 | 122.9 | 135.1 | 132.6 | 128.7 | 128.6 | 45.7 |
| | | | | | | | | |
| **Rd apo cyt c-b$_{562}$** | ALA 43 | 88.6 | 124.4 | 126.0 | 118.7 | 131.2 | 124.7 | 42.6 |
| | THR 44 | 116.1 | 105.8 | 119.7 | 130.2 | 128.7 | 130.1 | 24.4 |
| | LYS 47 | 168.6 | 149.3 | 139.8 | 132.8 | 131.0 | 126.5 | 42.1 |
| | SER 52 | 89.0 | 123.4 | 118.5 | 117.1 | 127.8 | 130.9 | 41.9 |
| | PRO 53 | 112.7 | 104.3 | 114.1 | 113.5 | 127.3 | 130.8 | 26.5 |
| | ASP 54 | 111.1 | 104.3 | 102.9 | 117.4 | 127.5 | 135.9 | 33.0 |
| | LYS 83 | 168.6 | 122.9 | 135.1 | 132.6 | 128.7 | 128.6 | 45.7 |

Based on a study of four heme proteins [cyt c-b$_{562}$, cyt c′, sw-Mb, and h-Cygb] [16], we presented evidence that in the *de novo* synthesis of a turning region, residues are preferentially selected such that the range of molecular volume values (representing purely repulsive, excluded volume effects) span a small range of Δ values (Δ = 39.1 Å$^3$) relative to the total range spanned (Δ = 167.7 Å$^3$) by the 20 amino acids. In Table 6, Δ is the *maximum* difference of molecular volume values for first- through seventh-nearest neighbors centered on residue i. The overall average for cyt c-b$_{562}$ is 36.3 Å$^3$ (36.6 Å$^3$ for the apo protein). These data reinforce our conclusion that in the *de novo* synthesis of proteins [21], minimization of steric interactions in turning regions is of fundamental importance.

Results comparing the role of Fe in influencing cyt c-b$_{562}$ unfolding (*vs* the apo protein) are more nuanced [9, 22-30]. Tables A5 and A6 list values of the two metrics [δ, *ratio*] for residues within 10 Å of the Fe atom for cyt c-b$_{562}$ and 10 Å of the "virtual" Fe atom in the apo protein. Three

stages of unfolding are displayed, the first stage (5-residue segments), the third stage (9- residue segments), and the sixth stage (15-residue segments). For each residue i, the value of the metric for each protein is listed, pairwise, with the residue for the cytochrome with the larger value in red. Residue pairs for residue i that correspond to different residues in the two proteins are in blue. For metric δ, cyt c-$b_{562}$ in the first, third and sixth stage of unfolding has a greater number of residues with values greater than those of the apo protein: 18, 16 and 18 *vs* 16, 16 and 7. In compiling these data, two residues with essentially the same value were not included. For the *ratio* metric (cyt c-$b_{562}$) in the first, third and sixth stages, the numbers of residues having values greater than the apo protein are 16, 16, and 14, respectively. Those numbers for the apo protein are, respectively, 16, 12 and 10.

Our finding that three of the four helical regions in the apo protein unfold before corresponding helical regions in the holoprotein is not surprising, as heme iron ligation would be expected to stabilize the native folded structure [31]; what is more, our model is in full accord with experimental investigations of thermal unfolding of apo and holo cytochrome $b_{562}$ [32, 33]. Turning to kinetics experiments, Eaton *et al*. [20, 26-30] presented evidence that Rd apo cyt $b_{562}$ folds in an apparent two-state manner with the absence of detectable folding intermediates. In earlier protein engineering studies, they suggested that the rate-limiting reaction step (RLS) involves the formation of the two middle helices, H2 and H3. Based on the identification of three discrete intermediates, they proposed that Rd apo cyt $b_{562}$ folds with an early RLS. They noted that intermediates are formed only after the initial RLS and concluded that these states are hidden and hence that folding appears to be a two-step kinetics process. In our analysis, the [δ, ratio] and [α, γ] data show that H2>H1; that is, the geometry of the interior helix H2 is more conserved (*i.e.*, native like) than the exterior helix, H1. If the *last* helix to unfold is the *first* to

fold along the landscape leading to the native structure, then folding the interior helix is the RLS for the apo protein. And, as seems likely, cyt $b_{562}$ and cyt c-$b_{562}$ follow similar paths, the interior helix would protect the heme from misligation, thereby accounting for experimental results [9, 17, 18] suggesting that these folding energy landscapes are minimally frustrated.

Acknowledgments

We thank Devarajan (Dave) Thirumalai for very helpful comments. Work at Caltech was supported by the NIH (DK019038) and the Arnold and Mabel Beckman Foundation. Support at Pomona College was provided by the Howard Hughes Medical Institute Research Program and a Sontag Research Fellowship Award.

**REFERENCES**


1. Onuchic JN, Wolynes PG (2004) Theory of protein folding: Curr Opin Struct Biol 14, 70 – 75. a

2. Saven JG, Wolynes, PG (1996) Local conformational signals and the statistical thermodynamics of collapsed helical proteins: J Mol Biol 257, 199-216.

3. Onuchic JN, Luthey-Schulten Z, Wolynes PG (1997) Theory of Protein Folding: The energy landscape perspective: Ann Rev Phys Chem 48, 545-600.

4. Wolynes, PG (2015) Evolution, energy landscapes and the paradoxes of protein folding: Biochimie 119, 218-230.

5. Lin X., Schafer NP, Lu W, Jin, SX, Chen M., Onuchic JN, Wolynes, PG (2019) Forging tools for refining predicted protein structures: Proc Natl Acad Sci USA 116, 9400-9409.

6. Chiti F, Dodson CM (2017) Protein Misfolding, Amyloid Formation, and Human Disease: A Summary of Progress Over the Last Decade: Annu Rev Biochem 86, 27-68.

7. Chung HS, EatonWA (2018) Protein folding transition path times from single molecule FRET: Curr Opin Struct Biol 48, 30-39.

8. Weinkam P, Pletneva EV, Gray HB, Winkler JR, Wolynes PG (2009) Electrostatic effects on funneled landscapes and structural diversity in denatured protein ensembles: Proc Natl Acad Sci USA 106, 1790 –1801.

9. Kimura T, Lee JC, Gray HB, Winkler JR (2009) Folding energy landscape of cytochrome $cb_{562}$: Proc Natl Acad Sci USA 106, 7834 –7839.

10. Guo Z, Thirumalai D (1996) Kinetics and Thermodynamics of Folding of a de Novo Designed Four-helix Bundle Protein: J Mol Biol 263, 323-343.

11. Buchete N-V, Straub JE, Thirumalai D (2004) Development of novel statistical potentials for protein fold recognition: Curr Opin Struct Biol 14, 225-232.

12. Buchete N-V, Straub, JE, Thirumalai D (2003) Anisotropic coarse-grained statistical potentials improve the ability to identify nativelike protein structures: J Chem Phys 118, 7658-71.

13. Denesyuk NA, Thirumalai D (2015) How do metal ions direct ribozyme folding? Nat Chem 7, 793-801.

14. Kozak JJ, Gray HB (2019) Stereochemistry of residues in turning regions of helical proteins: J Biol Inorg Chem 24, 879-888.

15. Kozak JJ, Gray HB, Garza-Lopez RA (2016) Cytochrome unfolding pathways from computational analysis of crystal structures: J Inorg Biochem 155, 44-55.

16. Kozak JJ, Gray HB, Garza-Lopez RA (2020) Funneled angle landscapes for helical proteins: J Inorg Biochem 208, 111091.

17. Wittung-Stafshede P, Lee JC, Winkler JR, Gray HB (1999) Cytochrome $b_{562}$ folding triggered by electron transfer: Approaching the speed limit for formation of a four-helix-bundle protein: Proc Natl Acad Sci USA 96, 6587-6590.

18. Faraone-Mennella J, Gray HB, Winkler JR (2005) Early events in the folding of four-helix-bundle heme proteins: Proc Natl Acad Sci USA 102, 6315-6319.

19. Faraone-Mennella J, Tezcan FA, Gray HB, Winkler JR (2006) Stability and folding kinetics of structurally characterized cytochrome c-$b_{562}$: Biochemistry 45, 10504-10511.

20. Feng HQ, Takei J, Lipsitz R, Tjandra N, Bai YW (2003) Specific nonnative hydrophobic interactions In a hidden folding intermediate: implications for protein folding: Biochemistry 42, 12461-12465.

21. Korendovych IV, DeGrado WF (2020) De novo Protein Design, a Retrospective. Quart Rev Biophys 53, E3.

22. Lin Y-W, Ni F-Y, Yang T-L (2009) Early events in thermal unfolding of apocytochrome $b_{562}$ and its double-cysteine mutant as revealed by molecular dynamics simulation: J Mol Struct 898, 82-89.

23. Manyusa S, Whitford D (1999) Defining folding and unfolding reactions of apocytochrome b5 using equilibrium and kinetic fluorescence measurements: Biochemistry 38, 9533-9540.

24. Wang T, et al. (2007) Probing the folding intermediate of Rd-apocytochrome $b_{562}$ by Protein engineering and infrared T-jump: Protein Sci 16, 1176-1183.

25. Wang LJ, Sun N, Terzyan S, Zhang XJ, Benson DR (2006) Histidine/tryptophan π-stacking interaction stabilizes the heme-independent folding core of microsomal

apocytochrome b5 relative to that of mitrochondrial apocytochrome b5: Biochemistry 45, 13750-13759.

26. Feng, HQ Vu ND, Zhou Z, Bai, YW (2004) Structural examination of ϕ-value analysis in Protein folding: Biochemistry 43, 14325-14331.

27. Choy WY, Zhou Z, Bai YW, Kay LE (2005) An 15N NMR spin relaxation dispersion study of the folding of a pair of engineered mutants of apocytochrome $b_{562}$: J Am Chem Soc 127, 5066-5072.

28. Feng H, Zhou Z, Bai YW (2005) A protein folding pathway with multiple folding Intermediates at atomic resolution: Proc Natl Acad Sci USA 102, 5026-5031.

29. Zhou Z, Huang YZ, Bai YW (2005) An on-pathway hidden intermediate and the early rate-Limiting transition state of Rd-apocytochrome $b_{562}$ characterized by protein engineering: J Mol Biol 352, 757-764.

30. Feng H, Takei J, Lipsitz N, Bai Y (2003) Specific non-native hydrophobic interactions in a hidden folding intermediate. Implications for protein folding: Biochemistry 42 12461-12465.

31. Tezcan, FA, Winkler JR, Gray HB (1998) Effects of Ligation and Folding on Reduction Potentials of Heme Proteins: J Am Chem Soc 120, 13383-13388.

32. Robinson CR, Liu Y, O'Brien R, Sligar SG, Sturtevant JM (1998) A differential scanning calorimetric study of the thermal unfolding of apo- and holo-cytochrome $b_{562}$: Protein Science 7, 961-965.

33. Robinson, CR, Liu Y, Thomson, JA, Sturtevant, JM, Stephen G. Sligar, SG (1997) Energetics of Heme Binding to Native and Denatured States of Cytochrome $b_{562}$: Biochemistry 36, 16141-16146.

**APPENDIX**

**Table A1:** Difference δ (in Å) of n-residue linear extension of triplets minus the distance between terminal α-carbons for cyt c-$b_{562}$. Average for helical regions (residues in parentheses).

| **Extension (n)** | **Helix 1 (2-20)** | **Helix 2 (22-41)** | **Helix 3 (45-49)** | **Helix 4 (55-81)** | **Helix 5 (83-106)** |
|---|---|---|---|---|---|
| 5 | 4.382 | 4.584 | 3.231 | 4.501 | 3.971 |
| 7 | 6.512 | 6.740 | 6.811 | 6.696 | 5.881 |
| 9 | 9.509 | 9.933 | 11.12 | 9.676 | 8.819 |
| 11 | 12.50 | 12.96 | 16.21 | 12.70 | 11.58 |
| 13 | 16.19 | 16.20 | 20.67 | 16.04 | 14.36 |
| 15 | 19.91 | 19.90 | 25.40 | 19.37 | 17.91 |

**Table A2:** Difference δ (in Å) of n-residue linear extension of triplets minus the distance between terminal α-carbons for Rd apo cyt $b_{562}$. Average for helical regions (residues in parentheses).

| **Extension (n)** | **Helix 1 (1-19)** | **Helix 2 (22-41)** | **Helix 3 (58-80)** | **Helix 4 (55-81)** |
|---|---|---|---|---|
| 5 | 4.459 | 4.141 | 4.419 | 3.995 |
| 7 | 6.228 | 6.634 | 6.320 | 6.219 |
| 9 | 8.424 | 9.809 | 9.379 | 9.095 |
| 11 | 11.00 | 12.72 | 12.13 | 12.10 |
| 13 | 13.78 | 16.14 | 15.07 | 14.91 |
| 15 | 15.81 | 19.68 | 18.39 | 18.72 |

**Table A3:** Ratio of n-residue linear extensions of triplets to the distance between terminal α-carbons for cyt c-$b_{562}$. Average for helical regions (residues in parentheses).

| **Extension (n)** | **Helix 1 (2-20)** | **Helix 2 (22-41)** | **Helix 3 (45-49)** | **Helix 4 (55-81)** | **Helix 5 (83-106)** |
|---|---|---|---|---|---|
| 5 | 1.697 | 1.725 | 1.466 | 1.723 | 1.640 |
| 7 | 1.651 | 1.709 | 1.650 | 1.714 | 1.579 |
| 9 | 1.768 | 1.830 | 1.939 | 1.818 | 1.781 |
| 11 | 1.845 | 1.940 | 2.292 | 1.906 | 1.809 |
| 13 | 2.075 | 2.141 | 2.476 | 2.137 | 1.817 |

| | | | | | |
|---|---|---|---|---|---|
| 15 | 2.183 | 2.238 | 2.586 | 2.136 | 2.062 |

**Table A4:** Ratio of n-residue linear extensions of triplets to the distance between terminal α-carbons for Rd apo cyt $b_{562}$. Average for helical regions (residues in parentheses).

| **Extension (n)** | **Helix 1 (1-19)** | **Helix 2 (22-41)** | **Helix 3 (58-60)** | **Helix 4 (83-106)** |
|---|---|---|---|---|
| 5 | 1.720 | 1.705 | 1.717 | 1.640 |
| 7 | 1.623 | 1.705 | 1.650 | 1.638 |
| 9 | 1.706 | 1.831 | 1.784 | 1.793 |
| 11 | 1.769 | 1.928 | 1.830 | 1.857 |
| 13 | 1.882 | 2.152 | 1.897 | 1.932 |
| 15 | 1.993 | 2.238 | 2.005 | 2.067 |

**Table A5.** Difference δ (in Å) in distance of n-residue linear extension of triplets minus the distance between terminal alpha carbons for residues within 10 Å of Fe. Red denotes larger value in pair.

| | n=5 | | n=9 | | n=15 | |
|---|---|---|---|---|---|---|
| Residue i | cyt c-$b_{562}$ | Rd apo cyt c-$b_{562}$ | | | | |
| LEU 3 | 6.091 | 4.354 | | | | |
| GLU 4 | 4.628 | 5.337 | | | | |
| ASP 5 | 4.733 | 3.674 | 12.46 | 8.143 | | |
| ASN 6 | 4.728 | 4.174 | 9.291 | 10.12 | | |
| **MET 7** | 4.379 | | 9.330 | | | |
| **TRP 7** | | 3.704 | | 8.273 | | |
| GLU 8 | 4.602 | 4.786 | 9.769 | 10.35 | 18.87 | 15.01 |
| THR 9 | 4.589 | 4.547 | 9.508 | 8.211 | 16.83 | 18.66 |
| LEU 10 | 5.020 | 6.144 | 9.618 | 9.580 | 16.88 | 14.24 |
| ASN 11 | 5.098 | 4.374 | 9.145 | 9.193 | 16.62 | 17.36 |
| ASP 12 | 4.953 | 4.413 | 9.405 | 10.57 | 16.60 | 15.36 |
| ALA 36 | 4.835 | 4.937 | 9.700 | 11.08 | 16.58 | 16.43 |
| ALA 37 | 4.801 | 4.164 | 9.761 | 9.248 | 16.03 | 17.88 |
| LEU 38 | 4.977 | 5.489 | 8.711 | 8.265 | 15.99 | 14.91 |
| ASP 39 | 4.582 | 4.475 | 8.618 | 7.759 | 17.04 | 16.23 |
| ALA 40 | 3.757 | 2.766 | 8.738 | 9.087 | 16.31 | 16.09 |
| GLN 41 | 3.683 | 2.658 | 9.253 | 8.176 | 17.74 | 17.62 |
| LYS 42 | 3.674 | 3.450 | 6.571 | 4.815 | 16.71 | 13.30 |
| ALA 43 | 2.348 | 0.672 | 4.959 | 6.297 | 16.86 | 15.33 |
| THR 44 | 0.453 | 0.052 | 10.41 | 9.242 | 18.62 | 16.50 |
| PRO 45 | 0.2064 | 3.501 | 9.169 | 7.250 | 22.01 | 17.73 |
| PRO 46 | 5.5627 | 5.035 | 8.592 | 7.980 | 25.04 | 19.76 |
| GLY 64 | 4.365 | 5.134 | 9.253 | 9.926 | 15.98 | 14.84 |
| PHE 65 | 4.006 | 5.572 | 8.244 | 8.701 | 16.72 | 16.30 |
| LEU 94 | 2.352 | 4.248 | 8.237 | 9.195 | 13.77 | 17.90 |
| LYS 95 | 2.611 | 4.761 | 7.686 | 8.487 | 16.17 | 16.14 |
| THR 96 | 4.160 | 4.445 | 7.717 | 8.262 | 13.11 | 14.45 |
| THR 97 | 3.993 | 3.818 | 5.544 | 9.401 | 15.21 | 16.10 |
| **CYS 98** | 4.984 | | 9.137 | | 14.77 | |
| **ILE 98** | | 3.832 | | 9.419 | | 17.53 |
| **ASN 99** | 2.685 | | 7.536 | | 19.04 | |
| **ARG 99** | | 4.611 | | 7.913 | | 16.35 |

| | | | | |
|---|---|---|---|---|
| ALA 100 | 4.894 | 4.927 | 9.385 | 7.236 |
| **CYS 101** | 3.332 | | 8.097 | |
| **HIS 101** | | 3.705 | | 8.879 |
| **HIS 102** | 4.345 | | 12.84 | |
| **ASN 102** | | 2.510 | | 9.653 |

**Table A6.** Ratio of n-residue linear extension of triplets to the distance between terminal alpha carbons for residues within 10 Å of Fe. Red denotes larger value.

| | n=5 | | n=9 | | n=15 | |
|---|---|---|---|---|---|---|
| Residue i | cyt c-$b_{562}$ | Rd apo cyt c-$b_{562}$ | 106 | apo 106 | 106 | apo 106 |
| LEU 3 | 1.981 | 1.718 | | | | |
| GLU 4 | 1.730 | 1.867 | | | | |
| ASP 5 | 1.773 | 1.556 | 2.190 | 1.643 | | |
| ASN 6 | 1.759 | 1.606 | 1.735 | 1.800 | | |
| **MET 7** | 1.700 | | 1.758 | | | |
| **TRP 7** | | 1.553 | | 1.673 | | |
| GLU 8 | 1.723 | 1.736 | 1.806 | 1.847 | 1.917 | 1.699 |
| THR 9 | 1.740 | 1.791 | 1.775 | 1.660 | 1.788 | 1.887 |
| LEU 10 | 1.850 | 2.146 | 1.781 | 1.741 | 1.797 | 1.646 |
| ASN 11 | 1.850 | 1.743 | 1.723 | 1.650 | 1.774 | 1.775 |
| ASP 12 | 1.825 | 1.649 | 1.765 | 1.867 | 1.778 | 1.733 |
| ALA 36 | 1.774 | 1.804 | 1.798 | 1.970 | 1.768 | 1.805 |
| ALA 37 | 1.794 | 1.623 | 1.807 | 1.788 | 1.683 | 1.815 |
| LEU 38 | 1.831 | 1.990 | 1.662 | 1.591 | 1.695 | 1.645 |
| ASP 39 | 1.738 | 1.740 | 1.650 | 1.577 | 1.721 | 1.683 |
| ALA 40 | 1.534 | 1.329 | 1.605 | 1.655 | 1.713 | 1.723 |
| GLN 41 | 1.502 | 1.345 | 1.690 | 1.587 | 1.772 | 1.765 |
| LYS 42 | 1.430 | 1.407 | 1.371 | 1.261 | 1.733 | 1.525 |
| ALA 43 | 1.247 | 1.062 | 1.278 | 1.388 | 1.712 | 1.614 |
| THR 44 | 1.035 | 1.004 | 1.755 | 1.634 | 1.884 | 1.717 |
| PRO 45 | 1.018 | 1.404 | 1.649 | 1.471 | 2.110 | 1.742 |
| PRO 46 | 1.866 | 1.734 | 1.550 | 1.502 | 2.587 | 1.945 |
| GLY 64 | 1.657 | 1.888 | 1.728 | 1.832 | 1.742 | 1.655 |
| PHE 65 | 1.619 | 2.067 | 1.627 | 1.670 | 1.787 | 1.762 |
| LEU 94 | 1.280 | 1.669 | 1.618 | 1.761 | 1.622 | 1.922 |
| LYS 95 | 1.326 | 1.779 | 1.643 | 1.668 | 1.739 | 1.776 |
| THR 96 | 1.617 | 1.721 | 1.545 | 1.626 | 1.576 | 1.638 |
| THR 97 | 1.828 | 1.560 | 1.390 | 1.773 | 1.659 | 1.785 |
| **CYS 98** | 1.812 | | 1.705 | | 1.682 | |
| **ILE 98** | | 1.545 | | 1.805 | | 1.889 |

| | | | | | | |
|---|---|---|---|---|---|---|
| **ASN 99** | 1.417 | | 1.618 | | 1.941 | |
| **ARG 99** | | 1.758 | | 1.589 | | 1.801 |
| ALA 100 | 1.778 | 1.883 | 1.729 | 1.538 | | |
| **CYS 101** | 1.440 | | | | | |
| **HIS 101** | | 1.528 | | | | |
| **HIS 102** | 1.641 | | | | | |
| **ASN 102** | | 1.343 | | | | |

**Declaration of interests**

☒ The authors declare that they have no known competing financial interests or personal relationships that could have appeared to influence the work reported in this paper.

☐The authors declare the following financial interests/personal relationships which may be considered as potential competing interests:

GRAPHICAL ABSTRACT (SYNOPSIS)

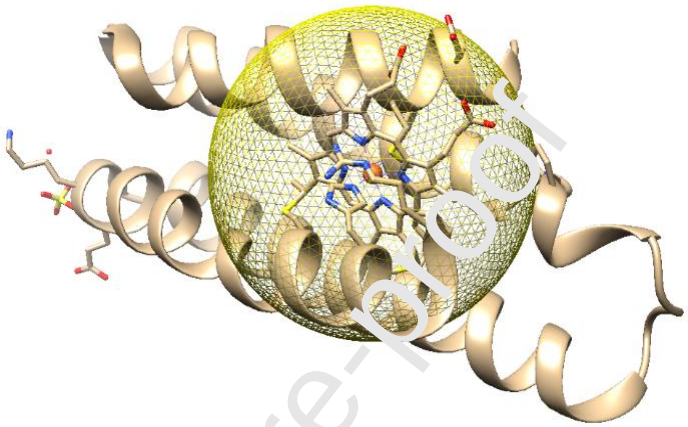

The folding landscape of cytochrome c-$b_{562}$ is minimally frustrated, owing to helix encapsulation of the heme.

HIGHLIGHTS

- Geometrical model to study unfolding of two cytochromes.
- Model quantifies the resiliency of the native state to steric perturbations.
- Development of angular phase diagrams.
- Sequential unfolding of helical regions is predicted.
- Percent departure of helical and non-helical regions is calculated.